Naval Research Laboratory

Washington, DC 20375-5320

Estimating the Effective Depth of Laser Imaging Systems in Various Ocean Environments

JERRY L. GORLINE
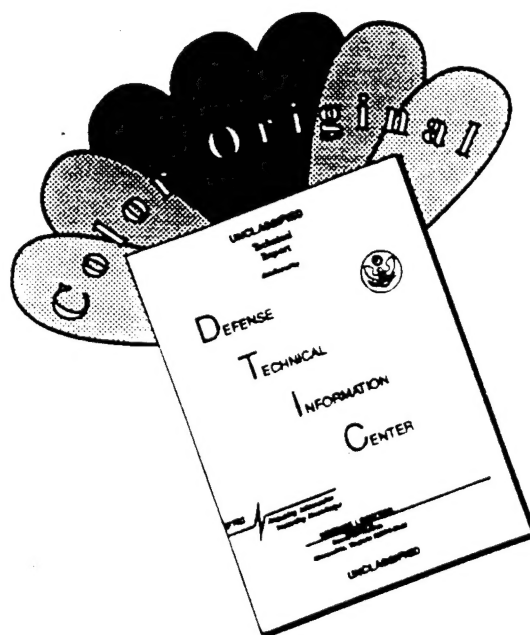
Advanced Information Technology Branch
Information Technology Division

May 9, 1996

19960627 018

DTIC QUALITY INSPECTED 1

DISCLAIMER NOTICE

THIS DOCUMENT IS BEST QUALITY AVAILABLE. THE COPY FURNISHED TO DTIC CONTAINED A SIGNIFICANT NUMBER OF COLOR PAGES WHICH DO NOT REPRODUCE LEGIBLY ON BLACK AND WHITE MICROFICHE.

REPORT DOCUMENTATION PAGE

Public reporting burden for this collection of information is estimated to average 1 hour per response, including the time for reviewing instructions, searching existing data sources, gathering and maintaining the data needed, and completing and reviewing the collection of information. Send comments regarding this burden estimate or any other aspect of this collection of information, including suggestions for reducing this burden, to Washington Headquarters Services, Directorate for Information Operations and Reports, 1215 Jefferson Davis Highway, Suite 1204, Arlington, VA 22202-4302, and to the Office of Management and Budget, Paperwork Reduction Project (0704-0188), Washington, DC 20503.

1. AGENCY USE ONLY (Leave Blank)	2. REPORT DATE May 9, 1996	3. REPORT TYPE AND DATES COVERED Final Report	

4. TITLE AND SUBTITLE

Estimating the Effective Depth of Laser Imaging Systems in Various Ocean Environments

5. FUNDING NUMBERS

6. AUTHOR(S)

Jerry L. Gorline

7. PERFORMING ORGANIZATION NAME(S) AND ADDRESS(ES)

Naval Research Laboratory
Washington, DC 20375-5320

8. PERFORMING ORGANIZATION REPORT NUMBER

NRL/FR/5580--96-9809

9. SPONSORING/MONITORING AGENCY NAME(S) AND ADDRESS(ES)

Commander, Naval Sea Systems Command
2531 Jefferson Davis Highway; Program Executive Office-Mine Warfare
Arlington, VA 22242-5167

10. SPONSORING/MONITORING AGENCY REPORT NUMBER

11. SUPPLEMENTARY NOTES

12a. DISTRIBUTION/AVAILABILITY STATEMENT

Approved for public release; distribution unlimited.

12b. DISTRIBUTION CODE

13. ABSTRACT (Maximum 200 words)

In this report we present the results of running Monte Carlo simulations on the Connection Machine (CM-5E) to study the behavior of laser propagation in the ocean. We developed an advanced hydrologic radiative transfer model to estimate the effective depth of a laser imaging system in various ocean environments. This model simulates a flat ocean surface. The effective depth is defined as that at which a six-pixel wide disk target can no longer be detected in the upward irradiance field at the ocean surface. Simulations showed that the effective depth was inversely proportional to the total attenuation coefficient.

14. SUBJECT TERMS Lidar imaging Ocean optics Parallel processing			15. NUMBER OF PAGES 30
			16. PRICE CODE

17. SECURITY CLASSIFICATION OF REPORT UNCLASSIFIED	18. SECURITY CLASSIFICATION OF THIS PAGE UNCLASSIFIED	19. SECURITY CLASSIFICATION OF ABSTRACT UNCLASSIFIED	20. LIMITATION OF ABSTRACT UL

CONTENTS

ESTIMATING THE EFFECTIVE DEPTH OF LASER IMAGING SYSTEMS IN VARIOUS OCEAN ENVIRONMENTS

1. INTRODUCTION

Laser propagation in the ocean is a time-dependent process. Current hydrologic radiative transfer models assume uniform solar illumination. The light field is in equilibrium and represents a time-independent process. The estimates provided by these models cannot be equated to a column of light that undergoes stretching in both time and space. The best method for modeling time-dependent light propagation is with the Monte Carlo method. Here, both the time dependence and multiple scattering from hydrosols can be accounted for. The Monte Carlo method is also well suited for modeling a wind-roughened ocean surface. Monte Carlo techniques are computationally intensive. By using the Connection Machine, the computational problem becomes tractable.

In this report, we present the results of running Monte Carlo simulations on the Connection Machine (CM-5E) to study the behavior of laser propagation in the ocean. We developed an advanced hydrologic radiative transfer model to estimate the effective depth of a laser imaging system in various ocean environments. This model simulates a flat ocean surface. We define the effective depth as that at which the light from a six-pixel wide target can no longer be detected in the upward irradiance field at the ocean surface. The model simulates a two-dimensional array of detectors just above the ocean's surface that digitize the upwelling light field into a pixel map. This map has a spatial resolution of six pixels over the target. The circular disk target has a reflectivity of 10%. The resulting simulated pixel map is displayed with the Advanced Visualization Systems (AVS) Image Viewer.

This model simulates two targets within the laser footprint at different depths. The target depths are increased in 1-m increments. When the reflected light from a target is no longer detected as a discernible disk, the depth for the target is recorded as the effective depth for that particular ocean environment. We use the inherent optical properties of seven measured ocean environments to simulate laser propagation in water with a wide range of turbidity levels. Table 1 gives the optical properties of the seven ocean environments used in our simulations.

Table 1 — Optical Properties of the Seven Ocean Environments

	a (m^{-1})	b (m^{-1})	c (m^{-1})	a/b
Env A	0.122	0.043	0.165	2.840
Env B	0.082	0.117	0.199	0.700
Env C	0.179	0.219	0.398	0.820
Env D	0.195	0.275	0.470	0.710
Env E	0.188	0.433	0.621	0.434
Env F	0.125	1.205	1.330	0.104
Env G	0.366	1.824	2.190	0.167

1

A relevant discussion of optical properties of the ocean is given by Jerlov [1]. These measured properties include the total attenuation coefficient (c), the total scattering coefficient (*b*), the absorption coefficient (*a*) and the Volume Scattering Function (VSF). These quantities are related in the following way:

$$a + b = c, \qquad b = 2\pi \int_0^\pi \beta(\theta) \times \sin\theta \times d\theta, \quad \text{where } \beta(\theta) \text{ is the VSF.}$$

Section 2 describes the Monte Carlo model. Section 3 presents the details of implementing the model on the CM-5E. Section 4 explains the results of simulations with different ocean environments. We compare simulations with the same total attenuation coefficient but with different scattering coefficients. We present a summary of results from a two-layered model used to simulate the ocean environment during a recent sea test of a Light Detection and Ranging (LIDAR) imaging system. An analysis of the diffuse attenuation coefficient (*K*) and its correlation with the absorption coefficient are given. Section 5 discusses how these results can be used to estimate system performance in different ocean environments and presents plans for future work.

2. DESCRIPTION OF THE MONTE CARLO HYDROLOGIC MODEL

This Monte Carlo hydrologic model keeps track of the path of approximately 250,000 photons as they propagate through the water column. Each photon is given an initial weight of one unit of energy. For a 250 mJ laser pulse, a weight of one unit would correspond to 1 μJ of energy. This definition represents a single laser pulse delivered to the ocean volume. The laser pulse duration is about 10 ns, and the wavelength of the light is in the blue-green region of the visible spectrum. The assignment of weights to each photon is a variance reduction technique used to decrease the number of replications required to obtain reasonable estimates. The actual number of photons in a 250 mJ laser pulse is about 7×10^{17}. With variance reduction we can obtain reasonable results with as little as 1×10^5 replications. We will now give an example to illustrate this point. Let us assume that during a simulation, 350 photons strike one of the disk targets. One method of accounting for 10% target reflectivity is to kill 90% of these photons and only allow 10% to reflect back up in the water column. Let us assume that all of these 35 photons make it back to the ocean surface, each with a weight of 0.9. The total reflected energy from the target is 35×0.9 or 31.5 μJ. Another method is to allow all 350 photons to propagate back towards the surface. Now we have 350 photons whose weights and positions are recorded. To account for 10% target reflectivity, we multiply the weight of each photon by 0.1. The weight of each photon is now 0.09. The total reflected energy is 350×0.09 or 31.5 μJ. The total energy for the second method is the same as with the first method. The advantage in using the second method is that the amount of information concerning the scattering is 10 times greater than with the first method.

2.1 Initialization and Propagation of Photons

This hydrologic radiative transfer model projects approximately 250,000 photons onto a flat-ocean surface, from a point 200 m above the surface, as a rectangular beam of uniform irradiance. The midpoint of the laser pulse is directed straight down representing a nadir shot. The beam is refracted at the flat air/ocean interface in accordance with Snell's law and is allowed to propagate through the water to some predetermined depth. Figure 1 is a schematic drawing of the simulation geometry. This representation is not drawn to scale. The drawing shows the beam projected onto the ocean surface. The surface in the model is flat but is represented as a wavy surface in the drawing for
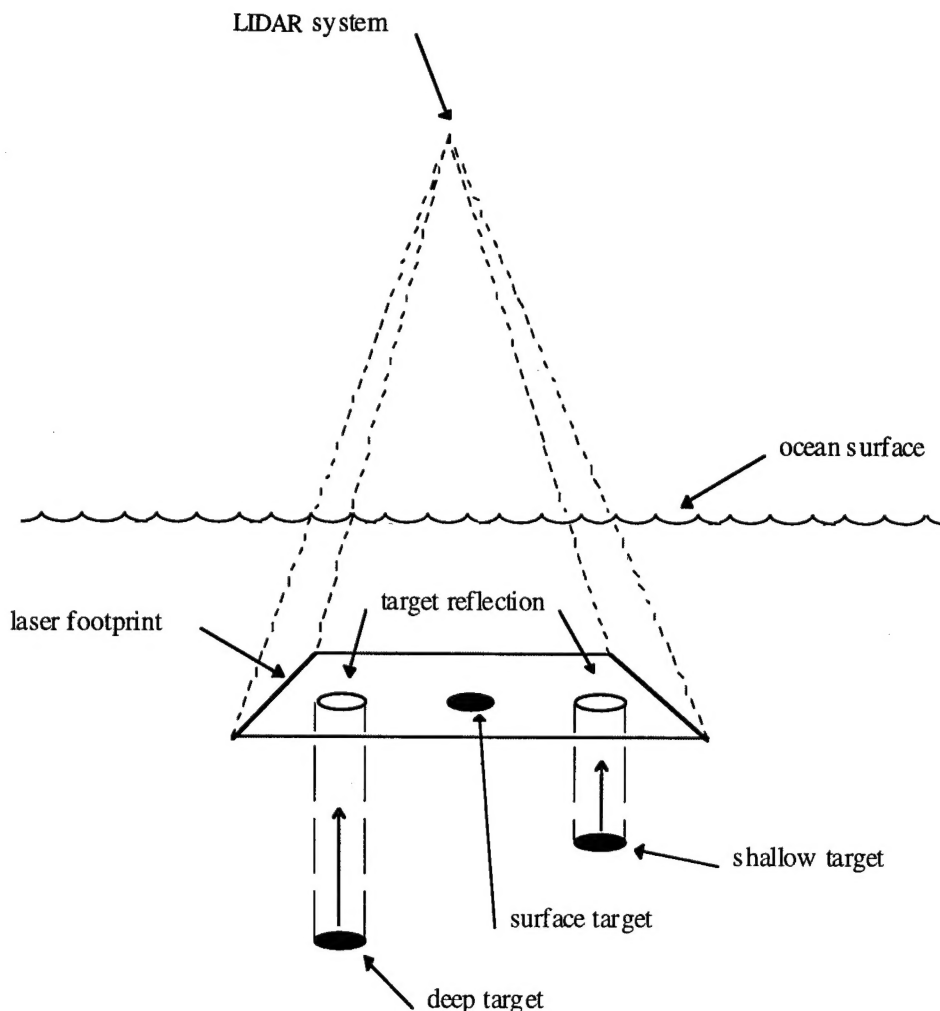
Fig. 1 — Schematic drawing of the simulation geometry (not drawn to scale)

aesthetic reasons. The footprint is rectangular in shape with the top defined as the right edge. There is a surface target in the center of the footprint, a shallow target at the top and a deeper target at the bottom. Photons that strike a disk target during the propagation are reflected back up towards the ocean surface. The weight and position of all photons that make it back to the ocean surface are digitized using a binning algorithm.

Multiple scattering from hydrosols is included during propagation. A more detailed description of the scattering algorithm is given by Gorline [2]. A brief description is given here. The distance to each scattering event is calculated by using a Monte Carlo inverse transform method. The probability of a scattering event is exponentially distributed. By inverting the cumulative distribution function for the probability of a photon scattering, the distance to the next scattering event can be calculated as

$$r = \frac{-\ell n(\varepsilon)}{b},$$

where r is the distance to next scatter, ε is a uniformly distributed random number in the interval from zero to one or $U(0,1)$ and b is the total scattering coefficient.

Once the photon is propagated to the next scattering event, the new photon direction is calculated using a Monte Carlo rejection technique. The new azimuthal angle is selected by drawing a uniformly distributed number between 0 and 2π, $U(0,2\pi)$. The azimuthal angle is independent of the polar angle. The new polar direction is drawn from a table that represents the VSF for a particular ocean environment. The rejection technique proceeds as follows. A uniformly distributed number between zero and π is drawn. Then, another uniformly distributed number between zero and the maximum y-value in the VSF table is drawn. These two values represent a point on a plot of the VSF vs polar angle. If the point falls below the VSF, we accept that angle as the new polar angle. If the point falls above the VSF, we reject that angle, draw another two numbers, and repeat the process. After selection of a new polar angle with the appropriate coordinate rotation, the photon is ready for propagation to the next scattering event.

2.2 Conditions for Terminating Photons

Photons propagate to each new scattering event until they reach a point of termination. Photons that strike a target are reflected back up towards the surface and the weight is reduced ten times to account for 10% reflectivity. The following four conditions cause a photon to be terminated:

1. A photon passes the depth of the deepest target.
2. A photon travels upward, back out of the water.
3. The weight of a photon falls below the threshold, which is $1 \times 10^{-4} \times e^{-ad_2}$, where a is the absorption coefficient, and d_2 is the depth of the second target.
4. A photon travels laterally too far away from the region of interest, which is the length or width of the footprint as measured from the center of the footprint.

Terminated photons that meet either condition one or two are saved by recording their position and weight. All processors with terminated photons are initialized with a new photon.

2.3 Development of the Volume Scattering Function

The VSF is an unnormalized probability distribution function for scattering angles. The VSF integrated over all solid angles gives the total scattering coefficient b. Our model uses VSFs measured by Petzold [3], with modifications between 170° to 180° described below. SRI International recently measured the VSF at 180°, a quantity also known as $\beta(\pi)$, during a sea test of a laser imaging system. This Beta Pi intrument is described by Maffione and Honey [4]. This SRI instrument was much more accurate near 180° than Petzold's instrument. Figure 2 compares SRI's measurement of $\beta(\pi)$ at two different depths with similar ocean environmental measurements taken by Petzold. The solid points in Fig. 2 are two VSFs measured by Petzold in the Bahamas. These measurements were taken 5 days apart in the same area and suggest that VSFs can shift vertically on the plot with time. This means that as turbidity increases in the water volume, the probability of a photon scattering any angle increases by about the same amount, as if the VSF is multiplied by a constant. The SRI_1 and SRI_2 points in Fig. 2 are measurements taken off the coast of Panama City Beach, FL, at the same time and at two different depths. The values at 170° were taken by the Applied Physics Lab (APL) using a backscatter meter similar to the one Petzold used. The values at 180° were measured by SRI using their Beta Pi instrument. These measurements were taken during a sea test of a laser imaging system in June 1994.

Measurements taken during the 2-week test showed a persistent two-layered structure in the optical properties of the water. There was a very clear layer extending from 13 m to the bottom that was about 25 m deep and a slightly more turbid layer above 13 m to the surface. The SRI_1 points
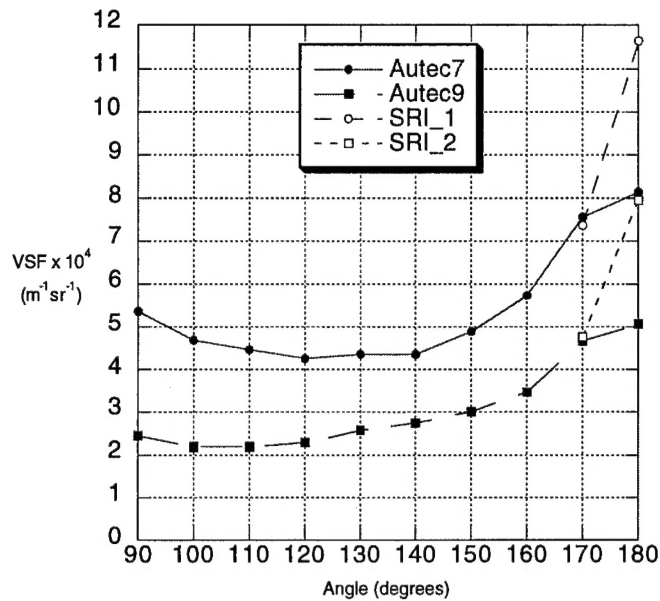
Fig. 2 — SRI's measurement of $\beta(\pi)$
was more accurate than Petzold's

in Fig. 2 that are higher on the vertical scale were measurements taken at a depth of 7 m. The SRI_2 points were measurements taken at a depth of 13 m. These measurements suggest that in layered ocean environments, the VSF can shift vertically on the plot with depth. We are using two VSFs measured by Petzold that compare well with the measurements taken by APL at 170°. The $\beta(\pi)$ measurements at 180° are about 40% higher than the Petzold measurements, suggesting a continuation of the upward trend in the slope from 170° instead of flattening out. For our model, we have adjusted Petzold's VSFs according to the SRI measurements.

Figure 3(a) shows the seven VSFs for angles less than 0.1°. The 4-digit numbers in the legend, divided by 1000, indicate the integrated value for each VSF. The VSFs given in Petzold's paper did not contain information for angles less than 0.1°. For angles less than 0.1°, the VSF values were manually extrapolated back to 0° and adjusted until the integral agreed with Petzold. The large increase near 0° is the result of the strong bias for forward scattering. Mie theory predicts a flattening out of VSFs near 0° but this behavior has not been measured in seawater. The continued upward slope near 0° could be due to turbulence [5]. Fluctuations in the index of refraction of the water cause light rays to deviate slightly in their paths. Similar fluctuations in the index of refraction of the air degrade the resolution of ground-based telescopes. This effect is well known to astronomers.

Another adjustment was made near 180° to more closely approximate measured backscattered light. Measurements of backscattered light from the ocean are typically significantly higher than predicted by Mie theory. This is known as the Enhanced Backscatter Effect (EBS). The mechanism responsible for part of this effect may involve constructive interference between similar light paths from transmitter to receiver [6]. This effect could only account for a factor of two increase in the amount of backscattered light. Small bubbles in the water have been shown to cause enhanced backscattering [7]. We adjusted the VSFs to simulate the EBS. In Fig. 3(b), we can see that the slopes of the VSFs increase dramatically starting at 179.9°. This feature was added manually to simulate a delta function near the backscatter angle.
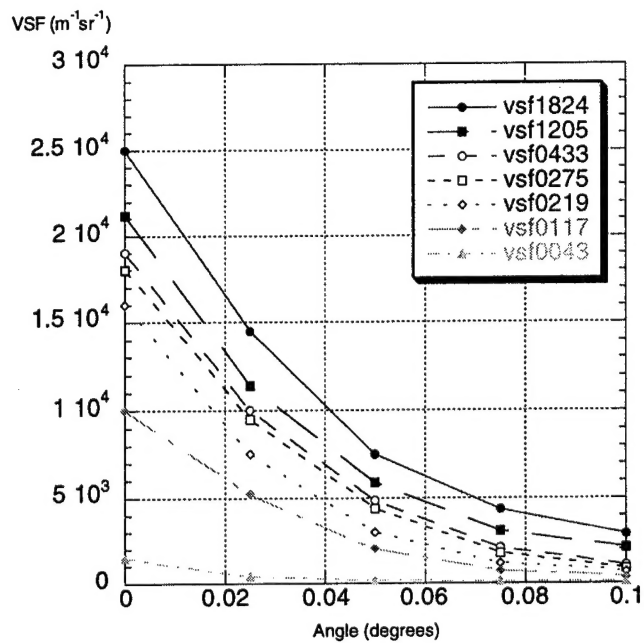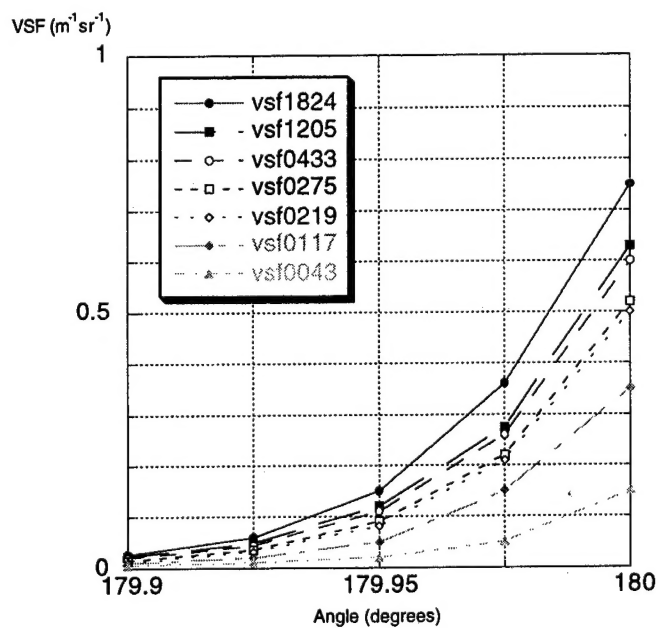
Fig. 3(a) — Seven VSFs near 0°

Fig. 3(b) — Seven VSFs near 180°

From these figures, we can see that the VSFs tend to be parallel to each other. These functions shift vertically on the plots as turbidity increases, as if the y-axis was scaled by a constant. There was one VSF that did cross the others. This VSF (vsf0433) was from seawater filtered in the laboratory to reduce turbidity and fell below vsf0275 between 0.2 and 0.1°. The other six VSFs were from measurements of seawater and did not cross each other. It is possible that the filtering process changed the distribution of hydrosols and resulted in lower VSF values near 0°. Reduced scattering near 0° could occur if the filtering process extracts more of the larger hydrosols and leaves the smaller ones behind. We needed a VSF to fill the gap between vsf0275 and vsf1205 and decided to make an additional adjustment upward in the lab-filtered VSF between 0.1 and 0.2° so that it would be more representative of seawater. This adjustment resulted in a slightly higher integrated value for the total scattering coefficient (b = 0.433 instead of b = 0.407). The other six VSFs were only adjusted between 0 and 0.1 and between 170 and 180°, and the integrated values for the total scattering coefficient was forced to be the same as Petzold's.

The VSF tables used in our simulations are the result of multiplying the VSF function by the sine of the angle:

$$table\_value(\theta) = \beta(\theta) \times \sin(\theta).$$

These tables are used in the Monte Carlo rejection technique for selection of photon-scattering angles. Numerical integration of the radiative transfer equation via Monte Carlo requires that we use the sin(VSF) rather than the VSF itself. Figure 4(a) gives the VSF table for angles close to 0°. Figure 4(b) gives the VSF table for angles close to 180° and shows a small local maximum near the backscatter angle. Without the simulated delta function, the VSF table showed no increase in the probability of a backscatter after multiplying by the sine of the angle. Adding the delta function is one method of simulating the EBS.

3. IMPLEMENTATION OF THE MODEL ON THE CM-5E

This algorithm is a Single Instruction Multiple Data (SIMD) implementation with the propagation synchronized over scattering events. The photons are propagated to each scattering event in parallel and all processors with terminated photons are reinitialized with new photons. This process continues until the number of replications exceeds 250,000. The photons that remain alive are then allowed to continue propagating until all have been terminated. For these stragglers, only processors with live photons continue the propagation. When all remaining photons are terminated, the loop ends and the results are saved in two output files. All photons that travel upward out of the water are saved as the upward irradiance at the ocean surface. All photons that pass the depth of the deepest target are saved as the downward irradiance at that depth.

3.1 Modeling the Photon Direction

The simulation initializes one photon in each processor. The photon x and y directions are uniformly distributed in the interval of the solid angle that subtends the laser footprint at the ocean surface. We use a three-dimensional directional unit vector called $U(x, y, z)$. Here,

$$U(x) = \frac{X\_Angle}{2} \times (2\varepsilon - 1),$$

$$U(y) = \frac{Y\_Angle}{2} \times (2\varepsilon - 1),$$

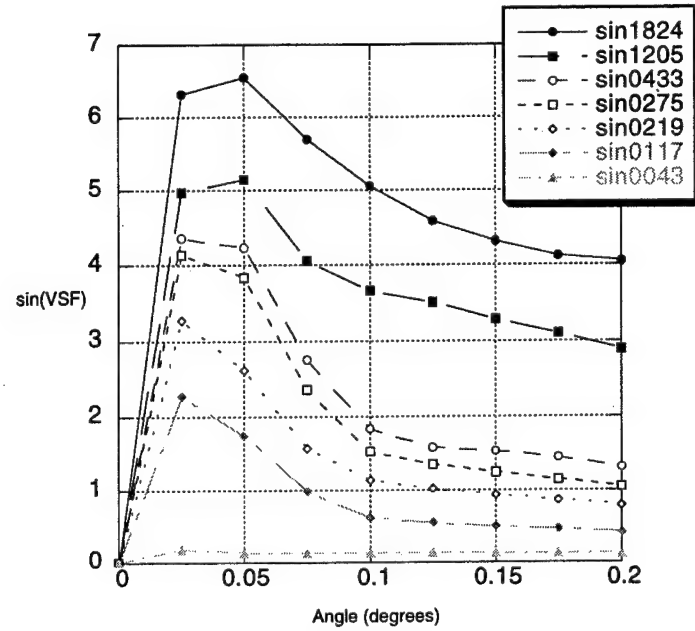$$U(z) = -\sqrt{1 - U(x)^2 + U(y)^2}.$$
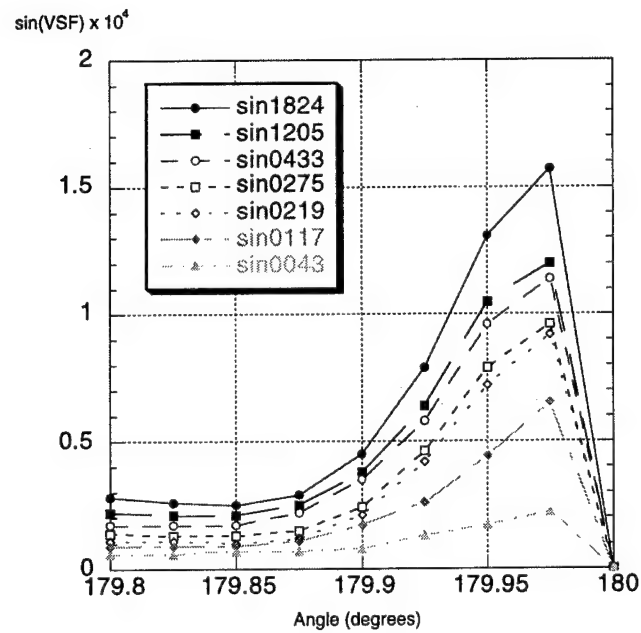
Fig. 4(a) — Sine of VSFs near 0°

Fig. 4(b) — Sine of VSFs near 180°

The vector $U(x, y, z)$ is normalized to ensure that the sum of the squares of the components is equal to unity with,

$$Norm = \sqrt{U(x)^2 + U(y)^2 + U(z)^2},$$

$$U(x) = \frac{U(x)}{Norm}, \qquad U(y) = \frac{U(y)}{Norm}, \qquad U(z) = \frac{U(z)}{Norm}.$$

Also, the vector components are parallel variables and the directions for photons in all processors are computed simultaneously. The negative sign for the z-direction means the photons are initially traveling downward. The X_Angle and Y_Angle are parameters that give the angular spread of the laser beam. The value ε is a uniformly distributed random number in the interval $U(0,1)$. All simulations were conducted with the laser looking straight down representing a nadir shot. For off-nadir shots, the y-direction would be shifted by the tangent of the scan angle or,

$$U(y) = \frac{Y\_Angle}{2} \times (2\varepsilon - 1) + \tan(Scan\_Angle).$$

3.2 Simulating Refraction at the Ocean Surface

The photons are projected to the surface using simple trigonometry and then refracted using Snell's Law. For refracting the photons, we used a method developed by Preisendorfer and Mobley [8]. We manipulate directional vectors instead of using trigonometric functions that require more computational resources. The equation for downward transmission from air to water is

$$\tilde{U}_t = \frac{1}{n_w}\left(\tilde{U} - c_1 \hat{n}\right), \qquad c_1 = \tilde{U} \cdot \hat{n} + \left[\left(\tilde{U} \cdot \hat{n}\right)^2 + n_w^2 - 1\right],$$

where

$\tilde{U}_t$ = the transmitted directional vector,

$\tilde{U}$ = the incident directional vector,

$\hat{n}$ = unit vector normal to the ocean surface, pointed up, for a flat ocean, $\hat{n} = (0,0,1)$,

n_w = index of refraction for water.

For upward transmission from water to air,

$$\tilde{U}_r = \frac{1}{n_w}\left(\tilde{U} - c_2 \hat{n}\right), \qquad c_2 = \tilde{U} \cdot \hat{n} - \left[\left(\tilde{U} \cdot \hat{n}\right)^2 + n_w^2 - 1\right].$$

The equation for upward or downward reflection is

$$\tilde{U}_r = \tilde{U} - 2\left(\tilde{U} \cdot \hat{n}\right)\hat{n},$$

where U_r = the reflected directional vector.

3.3 Tests to Terminate Weak or Uninteresting Photons

After photons are refracted, they propagate computationally in parallel to the first scattering event. Photons are tested to see if they have passed the first target. Photons that strike the first target are reflected upward. All other photons are tested to see if they have passed the second target. Photons that strike the second target are also reflected upward. All other photons that have passed the second target are terminated, extrapolated back to a plane parallel to the second target, and the positions and weights are recorded. The next test is to check for photons that have propagated back out of the water. For these photons, if the z-component of the directional vector is less than the cosine of the critical angle (0.66), the photons are reflected internally. This is the most efficient method of checking if the photon polar angle is greater than the critical angle. Photons traveling upward with a polar angle greater than the critical angle (48.5°) are internally reflected. We can see that photons entering the water have a harder time escaping into the air again. All other photons above the water are terminated, extrapolated back to the ocean surface, and the positions and weights are recorded.

Absorption is accounted for by adjusting the weight of each photon depending on how far it has traveled, or,

$$W_t = e^{-ra},$$

where W_t is the photon weight, r is the total distance traveled, and a is the absorption coefficient.

The weight of the photons that have struck a target are reduced by 90% to simulate 10% target reflectance. The last test is to terminate weak or uninteresting photons. All photons whose weight is less than the preset threshold or whose lateral distance exceeds the outlier distance are terminated. The threshold we set was $1 \times 10^{-4} \times e^{-ad_2}$, where a is the absorption coefficient, and d_2 is the depth of the second target. This allowed for the threshold to be set lower for environments with high absorption. The outlier distance was set to 40 m from the center of the laser footprint. This distance is well outside the region of interest, which is the length or width of the laser footprint as measured from the center of the footprint. For our simulations, the number of photons terminated because they fell below the threshold averaged less than 1%. The number of photons terminated as outliers averaged about 3 to 5%.

3.4 Recording Photon Positions and Weights

Photons that survive the above tests are allowed to continue propagating. The scattered direction is calculated and all processors with terminated photons are reinitialized with new photons. The scattered direction is calculated in parallel. Processors that have accepted a new polar angle have to wait until all the other processors make a selection before exiting the rejection routine. Then the photons are propagated to the next scattering event and the tests are conducted again. The procedure is repeated until the number of replications exceeds 250,000. Then a new loop is initiated where the stragglers are allowed to propagate until all are terminated. This section of the algorithm is inefficient (processors with terminated photons are idle) but necessary. It is important to let the stragglers run their course because they contain information in the wings of the distributions generated. When all the stragglers are finished, two output files are generated. One file contains the positions and weights of all photons that have propagated back out of the water. This file is labeled "up0" and represents the upward irradiance at the ocean surface. The second file contains the positions and weights of all photons that have passed the second target without striking it. This file is labeled "down2" and represents the downward irradiance at the depth of the second target.

3.5 Converting the Data into Pixel Maps

The irradiance files from the Monte Carlo simulation are read into a binning algorithm that converts the data into a pixel map. A detailed description of the binning algorithm is given in Carr et al. [9]. The area of interest is broken up into square pixel regions. The size of the squares are set so that six squares lined up end-to-end would be as wide as the target. The algorithm uses the photon's position to determine within which pixel the photon falls. The weights of the photons that fall within each pixel are summed to determine the energy value for that pixel. The pixel map generated by this process is read into the visualization application and viewed using the AVS Image Viewer.

3.6 Using AVS to Maximize SNR in the Pixel Maps

The AVS Imager has several features that allow the user to perform image enhancements. The colormap uses a rainbow scale to convert pixel values into color values. The color blue represents the lowest pixel values and red represents the highest. We adjusted the scale to enhance small changes close to the red end. The colormap also has threshold settings. The minimum threshold was set to zero. The maximum threshold was adjusted to give the maximum signal-to-noise ratio (SNR) in the image frame. We start with a low threshold that saturates all the pixels and slowly raise the threshold setting until maximum SNR is achieved. As the threshold increases, pixels that are not part of the target image turn blue. The maximum SNR is the threshold that results in the largest contrast between background noise (blue) and the target image (red). Table 2 gives the settings for each ocean environment. All of these settings resulted in target images that were clearly circular in shape and easy to see in pixel maps of targets above the effective depth. These settings increased as turbidity increased because the background noise also increased.

Table 2 — Maximum Threshold Settings
or the Seven Ocean Environments

	$c\ (m^{-1})$	threshold
Env A	0.165	0.0005
Env B	0.199	0.0100
Env C	0.398	0.0100
Env D	0.470	0.0150
Env E	0.621	0.0500
Eny F	1.330	0.1500
Env G	2.190	0.2500

4. SIMULATIONS IN DIFFERENT OCEAN ENVIRONMENTS

The first set of tests was conducted using the one-layer model in seven different ocean environments. Two disk targets were used to determine the effective depth. The shallow target was placed in the upper center portion of the laser footprint while the deeper target was placed in the lower center portion. We also placed a surface target in the middle center of the footprint to see how much the region below this target fills in at the depth of the deep target. See Fig. 1 for a schematic drawing of the simulation geometry. For each ocean environment, we ran a couple of simulations with targets at widely different depths to get a rough estimate of the depth at which the target image would no longer be visible. Then we ran simulations with targets above this rough estimate, increasing the depth by 1-m increments for each simulation. The two most turbid environments required 1/2-m increments to determine the effective depth because attenuation lengths for these environments ranged from 0.5 to 1 m. For these tests, the two targets were separated from each other by a depth of 3 m, except for the two most turbid environments, in which the targets were separated by a depth of

1.5 m. The upward irradiance data were used to determine the effective depth. Pixel maps of the upward irradiance at the ocean surface for three runs were compared visually using the AVS Image Viewer. The effective depth was the depth at which the target image was no longer a circular shape as observed with the Image Viewer. For clear water there was very little scattering, so the image stayed together longer until absorption reduced the SNR of the target. For more turbid water, scattering became the dominant factor in determining the effective depth.

4.1 Determining the Effective Depth in Different Ocean Environments

Figures 5 through 11 show the results of the simulations in the seven different ocean environments. The three panels in Figs. 5 through 11 are of the upward irradiance at the surface for different target depths. The reflection from the shallow targets are in the top part of the panel and the reflection from the deep targets are in the bottom part of the panel. The bottom three images are the corresponding downward irradiance at the depth of the deepest target. These images represent the total energy returning to the surface from one laser pulse delivered to the ocean volume. To be consistent with the definition of irradiance, these data should be divided by the laser pulse duration. Without dividing by the pulse duration, the data is really total energy (J) per unit area instead of energy density (W). Table 3 gives the optical properties of the seven ocean environments used in these simulations and the effective depth for each.

Table 3 — Optical Parameters of the Seven Ocean Environments,
with the Effective Depth

	a (m^{-1})	b (m^{-1})	c (m^{-1})	a/b	D_eff (m)
Env A	0.122	0.043	0.165	2.840	28
Env B	0.082	0.117	0.199	0.700	21
Env C	0.179	0.219	0.398	0.820	11
Env D	0.195	0.275	0.470	0.710	9
Env E	0.188	0.433	0.621	0.434	7
Env F	0.125	1.205	1.330	0.104	3
Env G	0.366	1.824	2.190	0.167	2

Figure 5 shows the results in the clearest water environment, which we called Env A. The depths of the targets for each of the three runs are given. The reflection for the target at 28 m (lower target image in Panel 2) is starting to lose its circular shape. This depth was selected as the effective depth. The image for the 29-m target was barely visible (lower target image in Panel 3). The scattering was minimal so the reflection images stayed together longer. Finally, absorption reduced the SNR enough for the target image to fade into the background. Figure 6 shows the results for Env B. The effective depth was 21 m. Scattering is beginning to cause more spreading in the image due to the higher turbidity.

Figure 7 shows the results for Env C. We are moving away from clear water, such as would be found around the Bahamas, to a medium turbid environment, such as offshore southern California. The optical properties of the first two environments (A and B) were measured by Petzold in the Bahamas. The optical properties of the next two environments (C and D) were measured by Petzold from offshore southern California. The effective depth for Env C was determined to be 11 m. Scattering is starting to dominate the image degradation process. The 12-m target image has spread to the point that it has faded into the background. Figure 8 shows that the effective depth is 9 m for Env D. Figure 9 shows an effective depth of 7 meters for Env E. Scattering continues to dominate the image degradation process. The optical properties of Env E were measured by Petzold from seawater

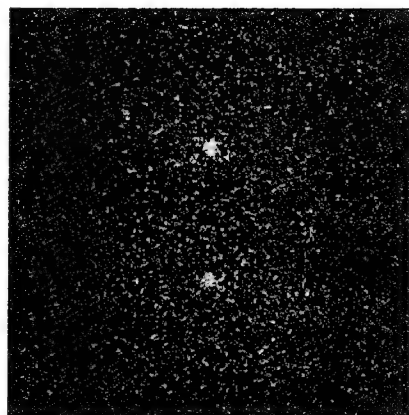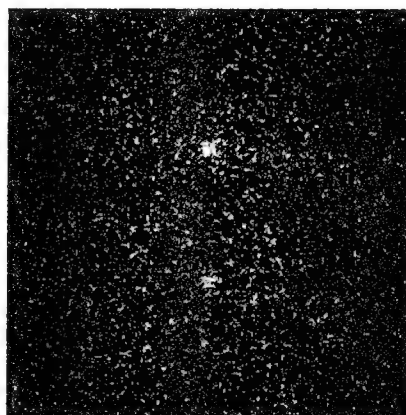Depth, Target 1: 24 m   25 m   26 m

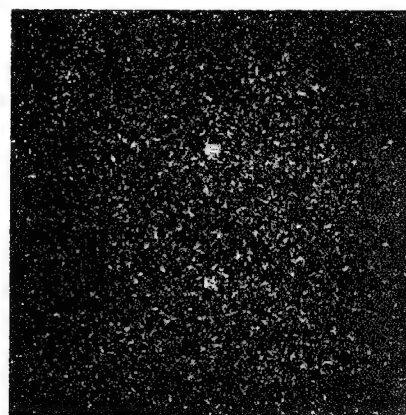Depth, Target 2: 27 m   28 m   29 m

Panel 1   Panel 2   Panel 3

Fig. 5 — Environment A, c = 0.165, D_eff = 11 m, threshold = 0.0005.
(The bottom image in Panel 2 is chosen as the target at the effective depth.)
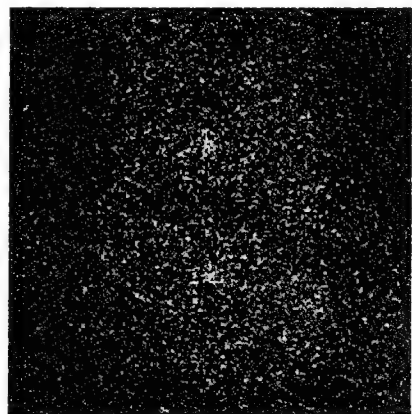
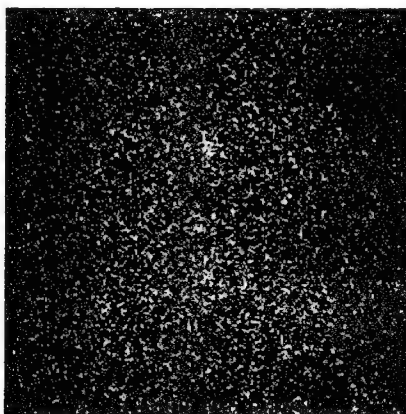Depth, Target 1: 17 m   18 m   19 m
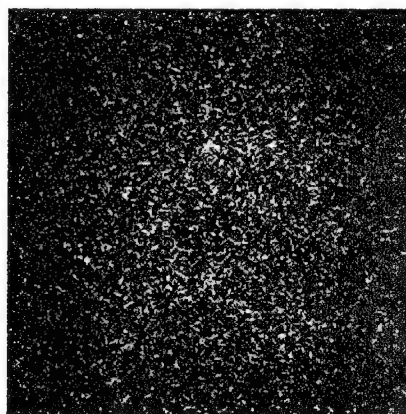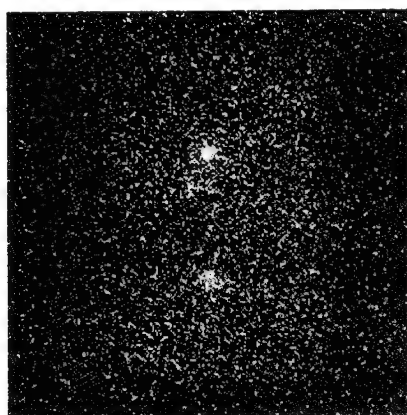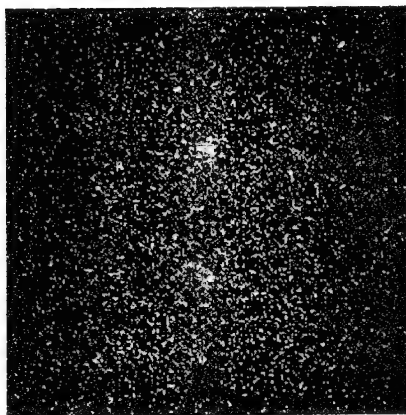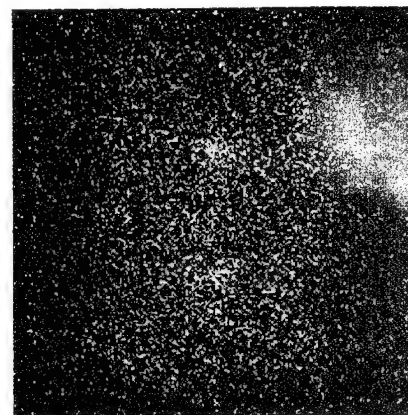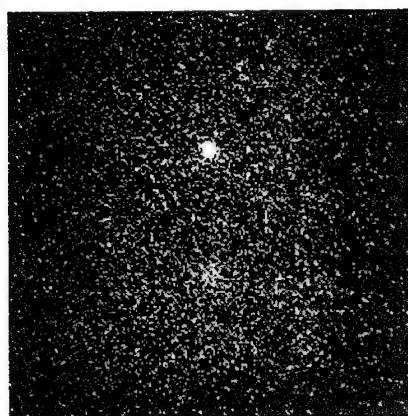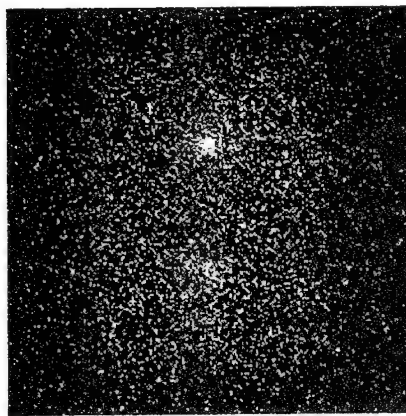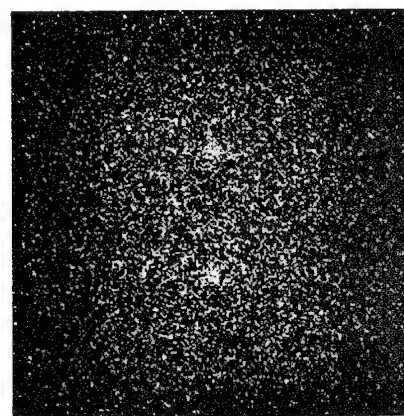
Depth, Target 2: 20 m   21 m   22 m

Panel 1   Panel 2   Panel 3

Fig. 6 — Environment B, c = 0.199, D_eff = 21 m, threshold = 0.01.
(The bottom image in Panel 2 is chosen as the target at the effective depth.)

Depth, Target 1: 8 m   9 m   10 m

Depth, Target 2: 11 m   12 m   13 m

Panel 1   Panel 2   Panel 3

Fig. 7 — Environment C, c = 0.398, D_eff = 11 m, threshold = 0.01.
(The bottom image in Panel 1 is chosen as the target at the effective depth.)

Depth, Target 1: 6 m   7 m   8 m

Depth, Target 2: 9 m   10 m   11 m

Panel 1   Panel 2   Panel 3

Fig. 8 — Environment D, c = 0.470, D_eff = 9 m, threshold = 0.015.
(The bottom image in Panel 1 is chosen as the target at the effective depth.)

filtered in a laboratory. For these last three ocean environments, the absorption coefficient (*a*) has remained almost constant while the total scattering coefficient (*b*) has increased from *b* = 0.22 to *b* = 0.43. The increased scattering causes the image to spread apart sooner as it propagates through the water column.

Depth, Target 1: 3 m   4 m   5 m

Depth, Target 2: 6 m   7 m   8 m

Panel 1   Panel 2   Panel 3
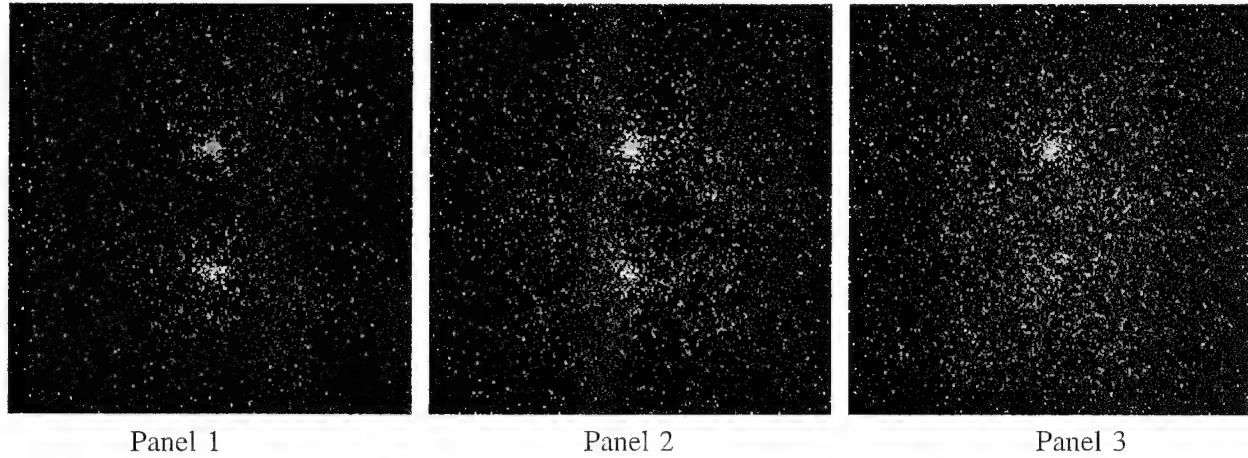
Fig. 9 — Environment E, *c* = 0.621, *D_eff* = 7 m, threshold = 0.05.
(The bottom image in Panel 2 is chosen as the target at the effective depth.)

Figures 10 and 11 represent turbid ocean environments commonly found in harbors and other littoral regions. These optical properties can also be found in lakes and rivers. The optical properties for these two ocean environments were measured by Petzold in San Diego harbor, California. Figure 10 shows that the effective depth is 3 m for Env F. Figure 11 shows an effective depth of 2 m for Env G. For the last two ocean environments, we are looking at attenuation lengths of 1 to 1.5 m. Consequently, the targets were separated from each other by a depth of 1.5 m instead of 3 m for the first five environments. The background is significantly higher as more light is scattered back out of the water than with the medium turbid water.

4.2 The Dependence of the Effective Depth on Turbidity

Figure 12(a) is a plot of the effective depth (D_{eff}) vs the total attenuation coefficient (c). This plot is compared with a curve generated using the function,

$$D_{eff} = \frac{4.24}{c},$$

where D_{eff} is the effective depth.

The constant 4.24 is obtained by computing a power law fit to the Monte Carlo data. Figure 12(b) shows a log-log plot of the data and the power law. In Fig. 12(a), the estimated effective depth for Env A falls slightly above the functional curve. Here the ratio of absorption to scattering is much higher than the other ocean environments. We will show later that scattering plays the dominant role in determining the effective depth. Having a higher scattering coefficient is much more significant in reducing the effective depth than having a higher absorption coefficient. The effective
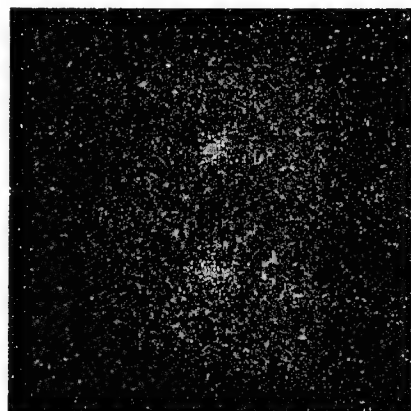
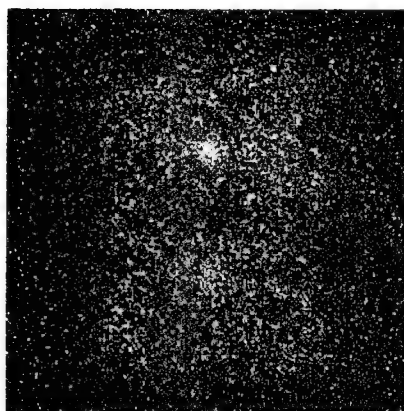Depth, Target 1: 1.5 m   2.0 m   2.5 m
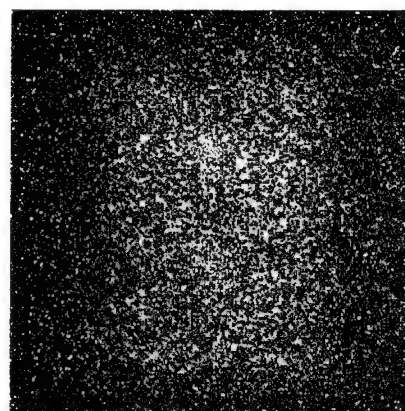
Depth, Target 2: 3.0 m   3.5 m   4.0 m

Panel 1   Panel 2   Panel 3

Fig. 10 — Environment F, c = 1.33, D_eff = 3.0 m, threshold = 0.15.
(The bottom image in Panel 1 is chosen as the target at the effective depth.)
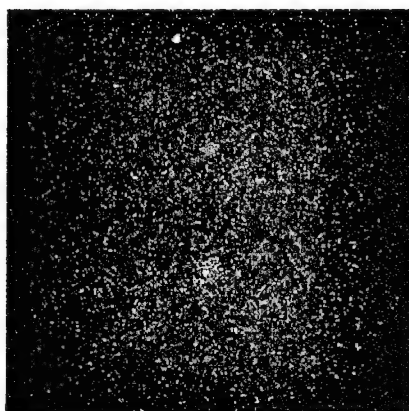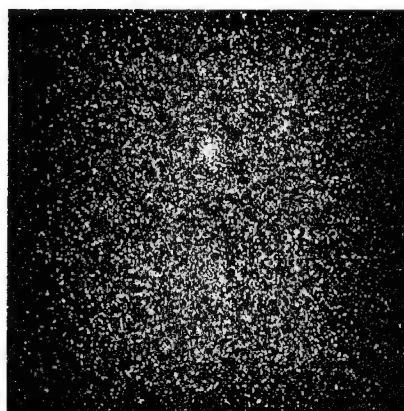
Depth, Target 1: 1.5 m   2.0 m   2.5 m
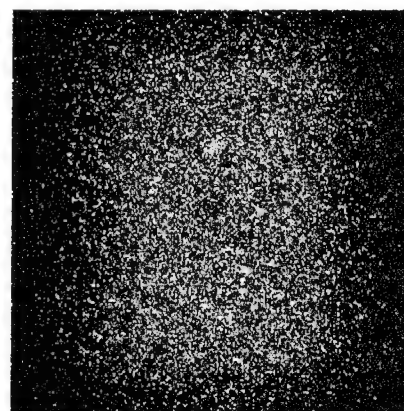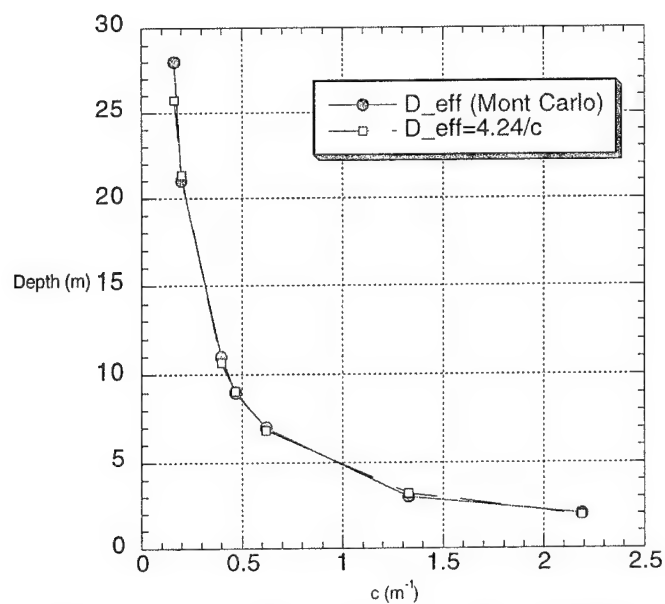
Depth, Target 2: 3.0   3.5 m   4.0 m

Panel 1   Panel 2   Panel 3

Fig. 11 — Environment G, c = 1.824, D_eff = 2.0, threshold = 0.25.
(The bottom image in Panel 1 is chosen as the target at the effective depth.)

Fig. 12(a) — The effective depth is inversely proportional
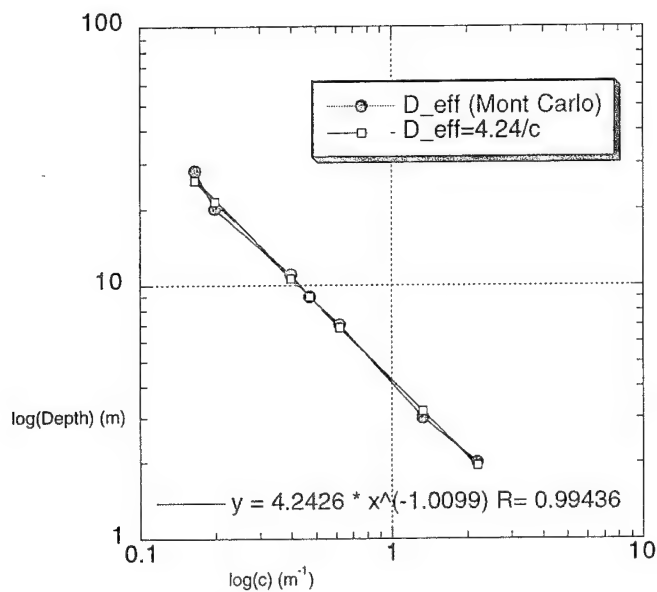to the total attenuation coefficient

Fig. 12(b) — Log-log plot of Fig. 12(a)

depth of the other ocean environments agree with the functional curve. We find that the effective depth is inversely proportional to the total attenuation coefficient. This result is reasonable since the inverse of the total attenuation coefficient is one attenuation length. We found that the effective depth is approximately four attenuation lengths.

Duntley [10] mentions the results of underwater visibility tests. For horizontal paths of sight, dark objects such as swimmers in black wet suits, can be observed up to a distance of $4/c$. These tests were conducted in a horizontal sighting range using solar illumination. Duntley states that this simple relationship does not hold when the path of sight is directed downward in the sea as sunlight is rapidly absorbed with depth. The Monte Carlo results suggest that this relationship does hold for laser light rather than for sunlight. We are assuming that the reflectivity of the wet-suits is about 10%. In Duntley's horizontal visibility test, the Sun is constantly supplying photons to the water volume between the swimmers and the observer. In a vertical visibility test, the solar illumination is significantly attenuated at a depth of $4/c$ and there is no additional input of photons. We are "photon starved" at this depth and the swimmers are not visible to the observer as in the horizontal test. For a laser imaging system, we are not photon starved at a depth of $4/c$, and the effective depth is similar to the results of the horizontal visibility tests.

4.3 Running Simulations with Higher a/b Ratios

We ran two tests to demonstrate the importance of scattering in determining the effective depth. The absorption coefficients of ocean environments B and D were increased so that the attenuation coefficients matched that of two measured ocean environments C and F. The effective depth for these altered environments were determined and compared with the measured ocean environments. Table 4 gives the parameters we used. Env C1 and Env F1 are the measured ocean parameters. Env C2 and Env F2 are environments with the altered parameters. The scattering coefficients for the altered environments are lower than for the measured environments. The thresholds for both altered environments were set to 0.0005. Figure 13 shows three runs with Env C2. The effective depth was 14 m. Figure 14 shows three runs with Env F2. The effective depth was 5.5 m. Figure 15 shows the effective depth from the seven measured ocean environments with the two altered environments added. We see that the effective depth of the altered environments are slightly deeper than the measured environments. The amount of scattering in the altered environments was significantly reduced and accounts for the better effective depth. This result explains why the effective depth of the clearest ocean environment fell above the curve $D_{eff} = 4.24/c$. The ratio a/b for Env A was 2.84. The ratio for the other environments ranged from 0.17 to 0.82. These two tests show that scattering is much more important than absorption in decreasing the effective depth. We decided to stay as close to the Petzold measurements as possible for the determination of the effective depth to simulate conditions in real ocean environments. A more controlled test would be to keep the ratio a/b or b/c constant for each ocean environment. Then we would be keeping the amount of absorption constant in each ocean environment.

Table 4 — Parameters for Comparing Oceans with the Same c and Different a and b

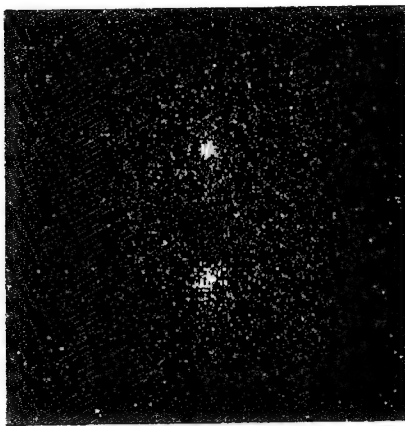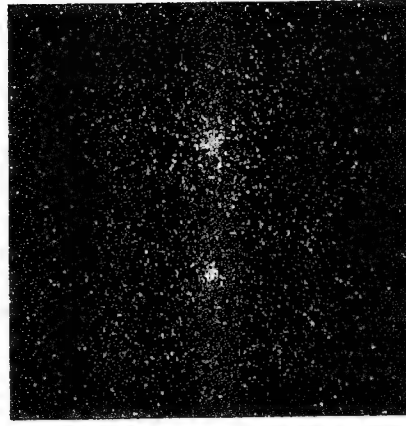|	a (m⁻¹)	b (m⁻¹)	c (m⁻¹)	a/b	D_eff (m)
Env C1	0.179	0.219	0.398	0.820	11
Env C2	0.281	0.117	0.398	2.400	14
Env F1	0.125	1.205	1.330	0.104	3
Env F2	0.897	0.433	1.330	2.070	5.5

Depth, Target 1: 10 m   11 m   12 m

Depth, Target 2: 13 m   14 m   15 m

Panel 1   Panel 2   Panel 3

Fig. 13 — Environment C2, c = 0.398, D_eff = 14 m, threshold = 0.0005.
(The bottom image in Panel 2 is chosen as the target at the effective depth.)
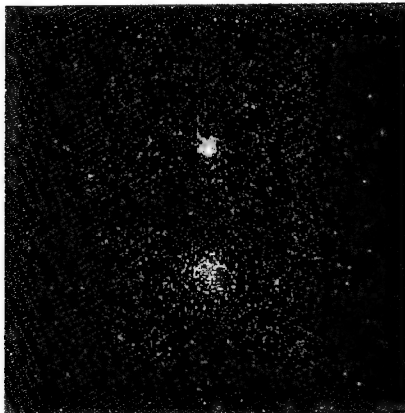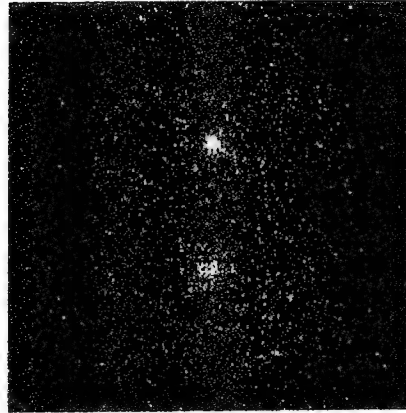
Depth, Target 1: 3.5 m   4.0 m   4.5 m
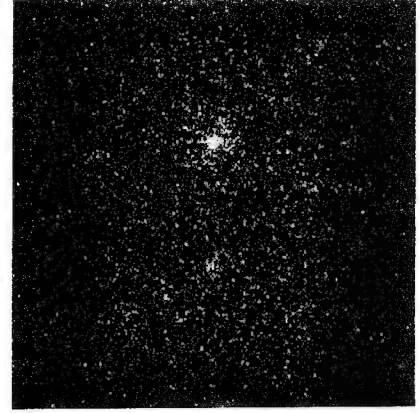
Depth, Target 2: 5.0 m   5.5 m   6.0 m

Panel 1   Panel 2   Panel 3

Fig. 14 — Environment F2, c = 1.33, D_eff = 5.5 m, threshold = 0.00005.
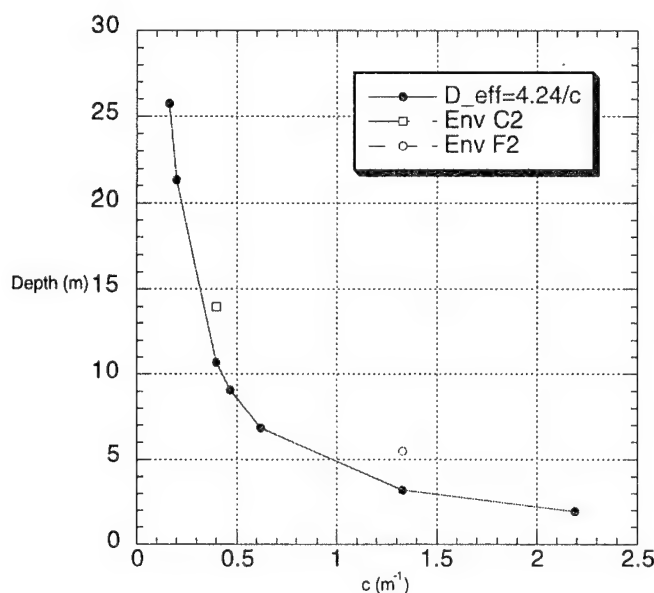(The bottom image in Panel 2 is chosen as the target at the effective depth.)

Fig. 15 — The effective depth of Env C2 and Env F2
compared with *Deff* = 4.24/c

4.4 Results Using a Two-Layered Model

A two-layered model was used next to simulate environmental conditions during a recent at-sea test of the Magic Lantern Advanced Development Model (ADM). The test was conducted by Coastal Systems Station (CSS), about 12 miles offshore from Panama City Beach, FL, between 20 June to 3 July, 1994. Environmental measurements taken during the test showed a two-layered structure in the optical properties of the water column. Figure 16 shows measurements of b and c that were taken during the Beta Pi measurement by SRI. The value for b was determined by measuring a and c and then subtracting a from c. The a and c measurements were taken by APL on 23 June. The sudden increase in b and c between 8 to 10 m is most likely a measurement error. The first layer extended from the surface to a depth of 13 m. The average values for the scattering coefficient and the attenuation coefficient were measured to be $b = 0.125$ and $c = 0.240$. The second layer started at 14 m and extended downward to near the bottom, which was about 25 m. This lower layer was clearer with $b = 0.042$ and $c = 0.115$. This two-layered structure persisted during the at-sea test.

To simulate the conditions during the sea test, we set the first target depth at 12 m and used a VSF similar to the measured conditions of the first layer. The parameters used to simulate the environment of the first layer were $a = 0.123$, $b = 0.117$, and $c = 0.240$. Then we used a VSF similar to the measured conditions of the second layer in the region below 12 m. The parameters used to simulate the environment of the second layer were $a = 0.072$, $b = 0.043$, and $c = 0.115$. We varied the depth of the second target in 1-m increments until the effective depth was determined. The algorithm was modified to simulate the layered ocean. All photons that passed 12 m using the first VSF were extrapolated back to 12 m, and a new distance to the next scattering event was calculated using the second VSF. This procedure can be done because an exponential process has no memory of the past. Photons that pass the first layer can be backed up to 12 m, and a new distance to the next scattering event can be calculated using the clearer ocean parameters of the second layer. Photons that upwell
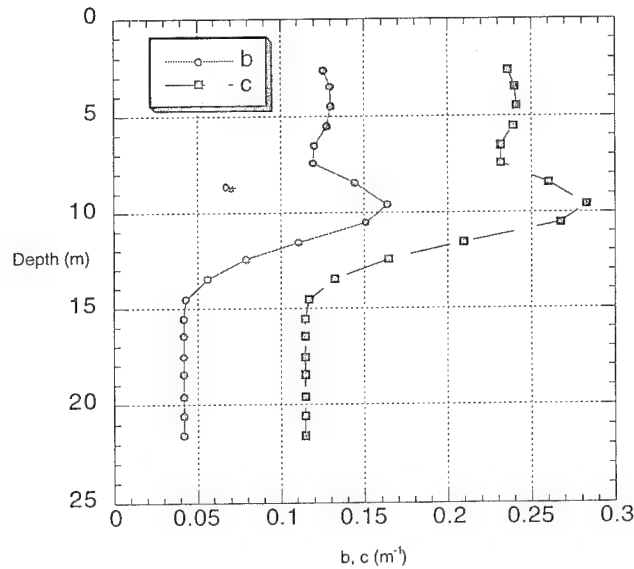
Fig. 16 — Measurement of b and c taken on 23 June 1994,
Panama City Beach, FL

from the second layer into the first layer are handled in a similar manner. We kept track of the total distance traveled in each layer separately. The weights of the finished photons were adjusted to account for absorption by multiplying the result of the effects of absorption in each layer. Here, $W_t = e^{-r_1 a_1} \times e^{-r_2 a_2} = e^{-(r_1 a_1 + r_2 a_2)}$, where r_1 is the total distance traveled in the first layer, a_1 is the absorption coefficient in the first layer, r_2 is the total distance traveled in the second layer, and a_2 is the absorption coefficient in the second layer.

Figure 17 shows the results of three runs using the two-layered model. The average attenuation coefficient was $c = 12/22 \, (0.24) + 10/22 \, (0.115) = 0.183$. The effective depth was determined to be 22 m. This depth is close to the effective depth for the one-layered model with $c = 0.199$. Figure 18 compares the computed curve as in Fig. 12(a), with the result of the two-layered model added. Results from the two-layered model compare well with those of the one-layered model.

4.5 Calculating the Diffuse Attenuation Coefficient

We used the downward irradiance data to estimate the diffuse attenuation coefficient (K) for all the ocean environments. Figure 19 is the downward irradiance data for Env B. Panel 1 is the downward irradiance at the ocean surface and shows the surface target in the center of the footprint. Panel 2 is the downward irradiance at the depth of the shallow target that is shown in the upper portion of the footprint. Panel 3 is the downward irradiance at the depth of the deeper target that is shown in the lower portion of the footprint. The shadow of the surface target and shallow target have partially filled in from multiple scattering. Figure 20 shows the downward irradiance fields at the depth of the deepest target for three different simulations of Env B. We can see that the downward irradiance decreases with depth.

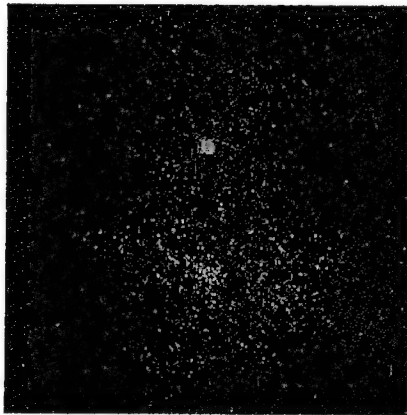Depth, Target 1: 12 m   12 m   12 m

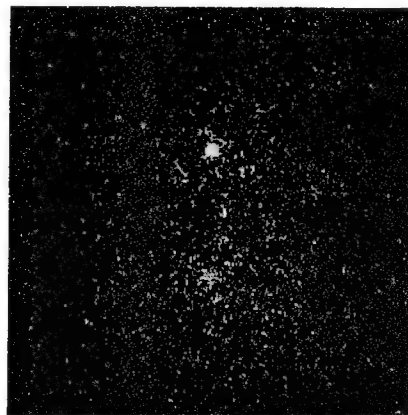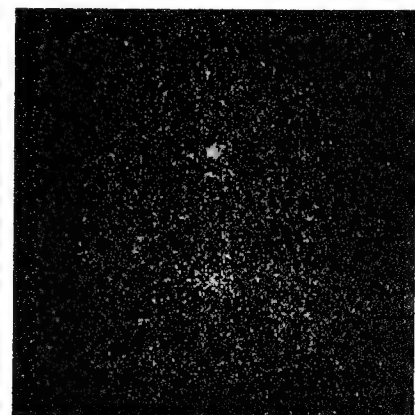Depth, Target 2: 21 m   22 m   23 m

Panel 1   Panel 2   Panel 3

Fig. 17 — Two-layered environment, c_ave = 0.183, D_eff = 22 m, threshold = 0.005.
(The bottom image in Panel 2 is chosen as the target at the effective depth.)

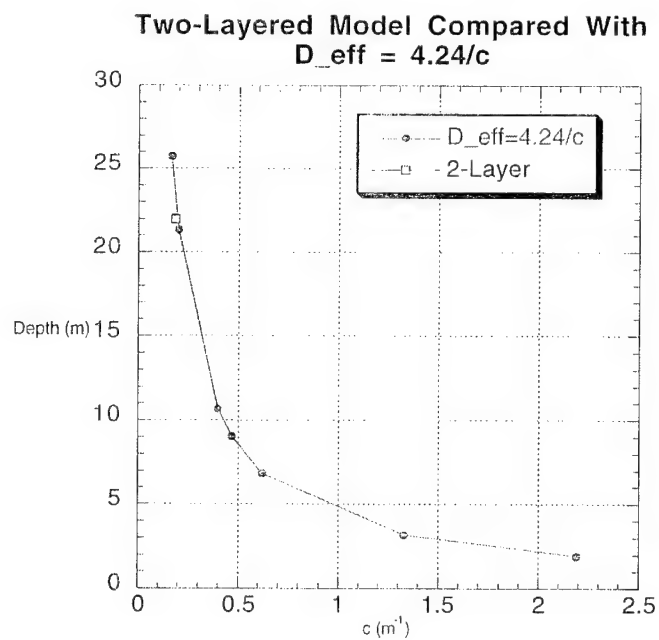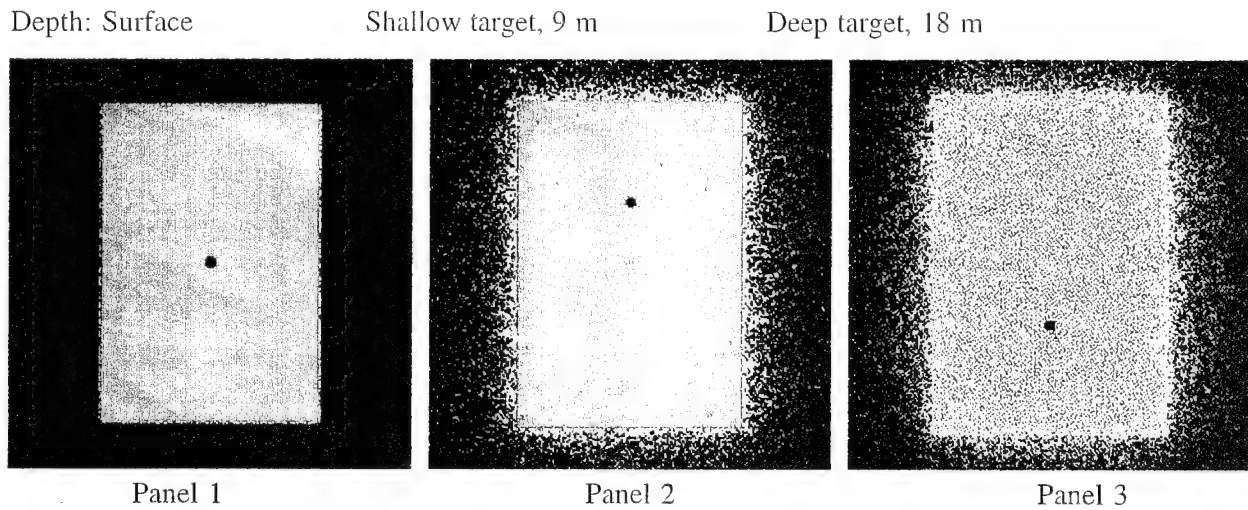Fig. 18 — The effective depth of the two-layered model
compared with $D\_eff = 4.24/c$

Depth: Surface   Shallow target, 9 m   Deep target, 18 m

Panel 1   Panel 2   Panel 3

Fig. 19 — Downward irradiance at three depths for one simulation

Depth: 19 m   20 m   21 m

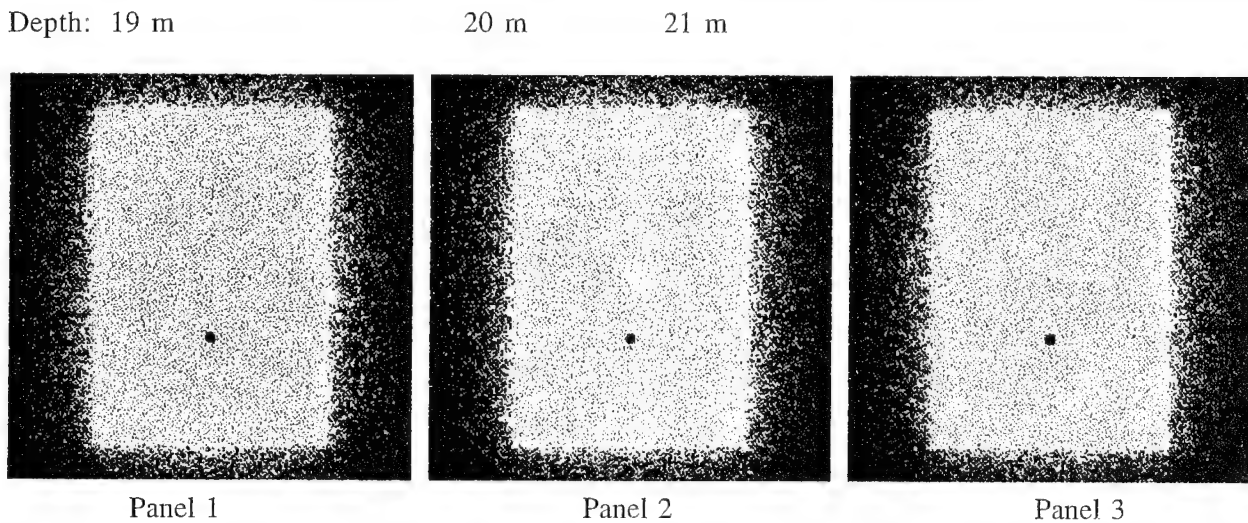Panel 1   Panel 2   Panel 3

Fig. 20 — Downward irradiance at three depths for three simulations

For each environment we calculated the average downward irradiance for every simulation. Then we plotted the natural log of the downward irradiance as a function of depth. The plots should be linear since, $E_1 = E_0 \times e^{-Kd}$, where E_1 is the average downward irradiance at depth d, E_0 is the average initial downward irradiance, K is the diffuse attenuation coefficient and d is the depth in meters.

Figure 21 is a semilog plot of the downward irradiance as a function of depth for Env A. We can see that data is linear indicating exponential behavior. The other seven ocean environments showed similar behavior. Table 5 shows the values for K and the average downward irradiance at the effective depth for each ocean environment. The downward irradiance is given in units of microjoules per meter squared ($\mu J/m^2$). Irradiance is usually given in units of watts per meter squared (W/m^2). To be consistent with the definition of irradiance we should divide by the duration of the laser pulse. Since this model simulates a single pulse event, we can define the laser pulse to be one second in duration. We could not find a relationship between K and the effective depth as we did with c. A more controlled test keeping the ratio a/b constant may show a relationship between K and
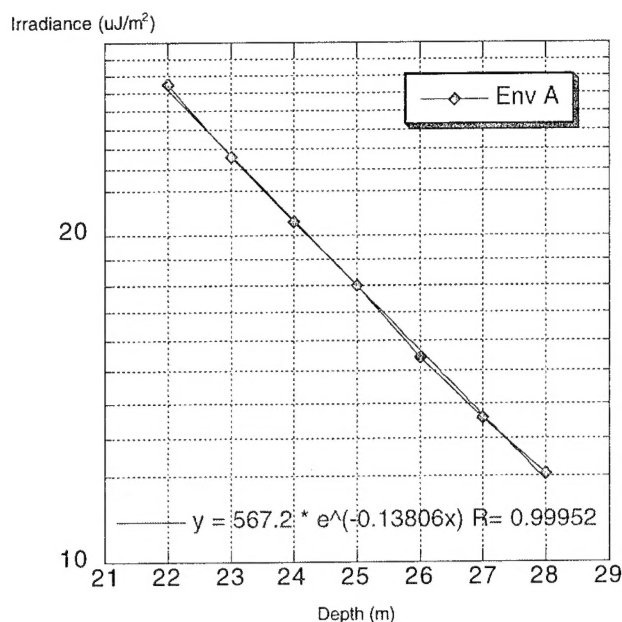
Fig. 21 — Average downward irradiance vs depth for Env A

Table 5 — *K* and the Average Downward Irradiance
at the Effective Depth

	a	K	c	E @ D_eff
Env A	0.122	0.138	0.165	12.06
Env B	0.082	0.110	0.199	63.71
Env C	0.179	0.207	0.398	59.82
Enc D	0.195	0.224	0.470	75.22
Env E	0.188	0.236	0.621	114.25
Env F	0.125	0.202	1.330	308.85
Env G	0.366	0.537	2.190	209.17

the effective depth. The diffuse attenuation coefficient is not a good measure of the amount of scattering occurring in the water column. Instead, K is highly correlated with the amount of absorption. Figure 22 shows a plot of a, K, and c for each ocean environment. We can see that the correlation between a and K is strong. Since scattering is more significant in degrading LIDAR system performance than is absorption, c is a better quantity for predicting system performance in turbid water than K.

5. CONCLUSIONS

Results from simulations using this hydrologic radiative transfer model show that the effective depth is inversely proportional to the total attenuation coefficient. This is a new but not unexpected result and compares well with Duntley's horizontal visibility tests. The effective depth for each environment was determined visually using the AVS display on a Sun workstation. Then the data
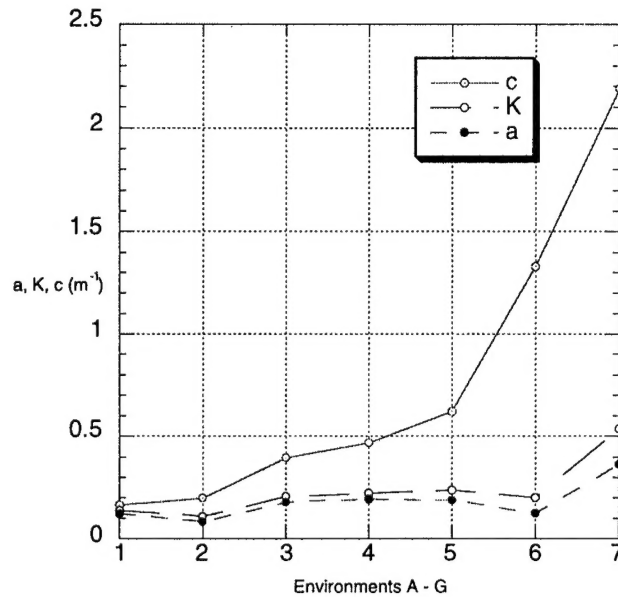
Fig. 22 — The diffuse attenuation coefficient (K) is correlated
with the absorption coefficient (a)

were analyzed to determine the depth dependence on turbidity. Some resolution was lost when converting from the display to color hardcopy. From the color pictures, it looks like the effective depth for Env B could be 20 m instead of 21 m and the effective depth for environment E could be 6 m instead of 7 m. A log-log fit of the data with the effective depth of Env B and Env E reduced by 1 m results in a slightly lower constant in the effective depth equation or $D_{eff} = 4.13/c$. This result is even closer to Duntley's tests but the fit to the data is not as good. These simulations do show a strong correlation with Duntley's $4/c$ dependence.

Since the product $D_{eff} \times c$ is constant, it would be reasonable to use this result to predict system performance in different ocean environments. This is possible if the system performance is known in one ocean environment. Suppose the performance depth of a LIDAR imaging system is measured to be 20 m in water where $c = 0.2$. If we want to estimate system performance in water where $c = 0.4$, we can use the following relation,

$$D_1 \times c_1 = D_2 \times c_2, \qquad D_2 = D_1 \times \frac{c_1}{c_2}, \qquad D_2 = 10m,$$

where

$D_1 = 20$ m, $c_1 = 0.2$ m^{-1}, and $c_2 = 0.4$ m^{-1}.

Here we find that the estimated performance depth of the system is 10 m in water where $c = 0.4$. These values were taken from Fig. 12(a) where $D_{eff} = 4.24/c$.

If we compare the increase of the absorption coefficient (a) and the total scattering coefficient (b) for all seven ocean environments, we find that (b) shows a larger range in values than does (a). The simulations show that scattering is the dominant process in image degradation. Absorption reduces the image irradiance but scattering spreads the image out over a wider area. Spreading causes

the image to fade into the background noise faster than the image being attenuated through absorption. The performance of a LIDAR imaging system is dependent on the signal-to-noise ratio (SNR) in the images received. Results from this model suggests that image spreading from scattering plays a much more significant role in reducing the SNR than attenuation from absorption. If this is true, image enhancement techniques, such as auto-focusing [9], would reduce image spreading from multiple scattering and increase the SNR in images obtained from turbid water environments.

5.1 Plans for Future Work

Plans for the future include simulating a spherical target instead of a disk target and incorporating off-nadir geometry into the model. The flat-ocean surface model can be extended to simulate a wind-roughened ocean surface. The wind-roughened surface can be modeled by using a hexagonal grid of triangular facets. The vertices of the hexagons are allowed to undulate to simulate waves on the ocean surface. The elevation angles of the vertices depends on the sea state and are drawn from an empirically derived distribution. The ray-tracing technique is tedious but straight-forward. This method is described in more detail by Preisendorfer and Mobley [7]. Since the laser pulse duration is in the nanosecond range, only one surface realization is needed for the entire simulation. The wind-roughened ocean surface model will be used to determine the performance of a laser imaging system as a function of sea state.

This hydrologic model has been designed to anticipate extensions such as a wind-roughened ocean surface. This model could be modified to provide input to a receiver model. The purpose of this research is to build a realistic model of laser propagation in the ocean. The author hopes that this model can be used in the future to build an end-to-end performance prediction model for LIDAR imaging systems.

6. ACKNOWLEDGMENTS

REFERENCES

1. N.G. Jerlov, *Marine Optics* (Elsevier Scientific Publishing Co., 1976).

2. Jerry L. Gorline, "Applying Monte Carlo Methods on the Connection Machine to Simulate Photon Propagation in the Ocean," NRL Memorandum Report 7377, 1993.

3. T.J. Petzold, "Volume Scattering Functions for Selected Ocean Waters," SIO Ref. 72-78, *Scripps Inst. Oceanogr.*, La Jolla, CA., 1972.

4. R.A. Maffione and R.C. Honey, "Instrument for Measuring the Volume Scattering Function in the Backward Direction," *SPIE's Int. Symp. on Opt. Appl. Sci. and Eng.*, 1992.

5. C.D. Mobley, *Light and Water* (Academic Press, San Diego, CA, 1994).

6. C.J. Solomon, "Double Passage Imaging Through Turbulence," *In Wave Propagation in Random Media (Scintillation)*, V.I. Tatarski, A. Ishimaru, V.U. Zavorotny, eds. (Institute of Physics Publishing, 1993), pp. 200-215.

7. W.P. Arnott and P.L. Marston, "Optical Glory of Small Freely Rising Gas Bubbles in Water: Observed and Computed Cross-Polarized Backscatter Patterns," *J. Opt. Soc. Am. A.* **5**(4), 496.

8. R.W. Preisendorfer and C.D. Mobley, "Unpolarized Irradiance Reflectances and Glitter Patterns of Random Capillary Waves on Lakes and Seas by Monte Carlo Simulation," NOAA Tech. Memo. ERL PMEL-63, 1985.

9. D.B. Carr, R.J. Littlefield, W.L. Nicholson, and J.S. Littlefield, "Scatterplot Matrix Techniques for Large N," *J. Amer. Statist. Assoc.* **82**, 424-436 (1987).

10. S.Q. Duntley, "Light in the Sea," *J. Opt. Soc. Amer.* **53**, 229 (1963).